Atlantic Tropical Cyclogenesis: A Three-Way Interaction between an African Easterly Wave, Diurnally Varying Convection, and a Convectively Coupled Atmospheric Kelvin Wave

MICHAEL J. VENTRICE, CHRISTOPHER D. THORNCROFT, AND MATTHEW A. JANIGA

Department of Atmospheric and Environmental Science, University at Albany, State University of New York, Albany, New York

(Manuscript received 20 May 2011, in final form 14 October 2011)

ABSTRACT

This paper explores a three-way interaction between an African easterly wave (AEW), the diurnal cycle of convection over the Guinea Highlands (GHs), and a convectively coupled atmospheric equatorial Kelvin wave (CCKW). These interactions resulted in the genesis of Tropical Storm Debby over the eastern tropical Atlantic during late August 2006. The diurnal cycle of convection downstream of the GHs during the month of August is explored. Convection associated with the coherent diurnal cycle is observed off the coast of West Africa during the morning. Later, convection initiates over and downstream of the GHs during the afternoon. These convective features were pronounced during the passage of the pre-Debby AEW. The superposition between the convectively active phase of a strong CCKW and the pre-Debby AEW occurred shortly after merging with the diurnally varying convection downstream of the GHs. The CCKW–AEW interaction preceded tropical cyclogenesis by 18 h. The CCKW provided a favorable environment for deep convection. An analysis of high-amplitude CCKWs over the tropical Atlantic and West Africa during the Northern Hemisphere boreal summer (1979–2009) highlights a robust relationship between CCKWs and the frequency of tropical cyclogenesis. Tropical cyclogenesis is found to be less frequent immediately prior to the passage of the convectively active phase of the CCKW, more frequent during the passage, and most frequent just after the passage.

1. Introduction

Atlantic tropical cyclones over the main development region (MDR; 5°–25°N, 15°–65°W) are commonly associated with African easterly waves (AEWs; e.g., Carlson 1969a; Zipser and Gautier 1978; Avila and Pasch 1992; Berry and Thorncroft 2005). For the July–September (JAS) months between 1979 and 2001, 85% of all AEWs (603) that propagated over the tropical Atlantic never developed into a tropical cyclone, highlighting the importance of determining the factors responsible for development (see Hopsch et al. 2010). The genesis of Tropical Storm Debby, associated with the second AEW during the National Aeronautics and Space Administration (NASA) African Monsoon Multidisciplinary Analyses (NAMMA) field campaign (Zawislak and Zipser 2010), was extremely difficult to forecast over the eastern Atlantic. According to the National Hurricane Center's (NHC) postseason tropical cyclone summary, the genesis of Debby occurred more rapidly than anticipated by the Tropical Weather Outlook products. The prediction of a developing tropical cyclone was issued only 3 h prior to genesis. The lack of warning is explained by the fact that the pre-Debby AEW was quite weak over Africa just prior to tropical cyclogenesis (e.g., Zawislak and Zipser 2010). This paper investigates the key processes that contributed to the rapid nature of the tropical cyclogenesis. These processes include an interaction between the AEW and diurnally varying convection at the West African coast and a strong convectively coupled equatorial atmospheric Kelvin wave (CCKW) over the eastern tropical Atlantic.

AEWs, the dominant synoptic weather systems observed over Africa and the tropical Atlantic during Northern Hemisphere boreal summer, are westward-propagating tropical waves that grow along the African easterly jet (AEJ) (e.g., Reed et al. 1977; Thompson et al. 1979; Avila and Pasch 1992; Mekonnen et al. 2006). Before reaching the coast of West Africa, the AEWs that

Corresponding author address: Michael Ventrice, University at Albany, State University of New York, 1400 Washington Avenue, Albany, NY 12222.
E-mail: mv945965@albany.edu

DOI: 10.1175/MWR-D-11-00122.1

later develop into tropical cyclones have a distinctive cold-core structure below the level of the AEJ, consistent with a vorticity maximum at the level of the AEJ (e.g., Reed et al. 1977; Kwon and Mak 1990; Hopsch et al. 2007). They often begin to transform toward more warm-core structures as they move toward the Guinea Highlands (GHs) region (5°–13°N, 8°–15°W) with regions of deep convection becoming more confined to the trough (Hopsch et al. 2010).

The GHs region was highlighted in Berry and Thorncroft (2005) and Hopsch et al. (2010) as an influential area for the amplification of AEWs, which may increase the likelihood of east Atlantic tropical cyclogenesis. They found that convection triggered over the elevated terrain of the GHs tends to generate low-level potential vorticity (PV), which merges with PV associated with an AEW during the wave passage. This PV merging process might play a critical role in enhancing AEWs propagating over the region. The low-level PV signature is also evident in the appearance of a low-level AEW track at the latitude of the GHs near the coast in addition to a second track over land north of the AEJ (Thorncroft and Hodges 2001).

The GHs region is composed of a series of elevated topographic features located in tropical West Africa, separating a portion of sub-Saharan Africa from the eastern tropical Atlantic. A Tropical Rainfall Measuring Mission (TRMM) 3B42 August daily average rainfall rate greater than 16 mm day^{-1} occurs just downstream of the elevated topography of the GHs region (Fig. 1). This exceptional rainfall rate downstream of the GHs region signifies that this area is one of the wettest places on the continent during boreal summer.

Zawislak and Zipser (2010) used infrared (IR) and microwave satellite imagery to observe the convection during the hours prior to classification of Debby. They suggest that a "GHs region type" genesis helps to explain the formation of Debby. Chiao and Jenkins (2010) performed a modeling study to explore the processes that influenced the genesis of Tropical Storm Debby. They also concluded that the GHs region played an important role by modulating the low-level westerly flow that deflected northward along the GHs. This deflection enhanced the low-level cyclonic circulation there and transported moist air toward the north, supporting the development of mesoscale convective systems (MCSs).

The above studies suggest the importance of understanding the convection generated in the vicinity of the GHs region for downstream tropical cyclogenesis. In this regard, this should include consideration of the role played by the coherent diurnal cycle, known to be dominant in the GHs region (Mekonnen et al. 2006). Past

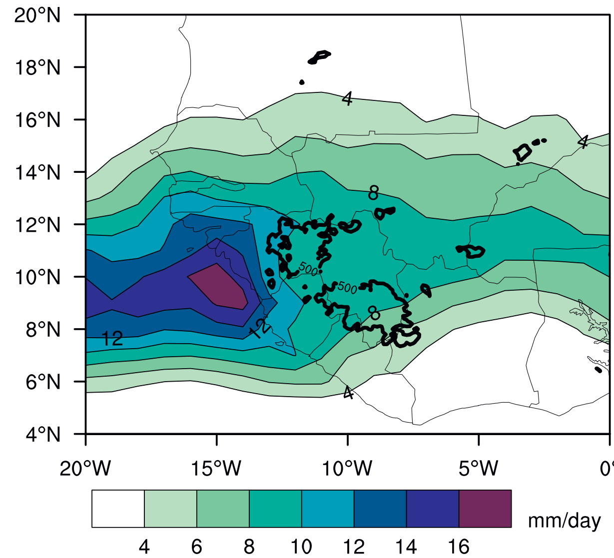

FIG. 1. August 1998–2009 averaged TRMM 3B42 rainfall rate (mm day^{-1}) is shaded and elevation (m) is contoured. Shade interval is 2 mm day^{-1}; contour interval is 500 m.

work suggests that convection is generally triggered close to the topography during the late afternoon in the vicinity of the GHs (e.g., Hodges and Thorncroft 1997; Yang and Slingo 2001; Laing et al. 2008). In contrast, an early morning peak in convection is expected over the ocean (e.g., Janowiak et al. 1994). The extent to which interactions between AEWs and the diurnal cycle are important for downstream tropical cyclogenesis is unknown.

Along with the convection generated over the GHs region, this paper will provide evidence that the pre-Debby AEW formed into a tropical cyclone during the superposition with a strong CCKW. CCKWs are eastward propagating tropical convective disturbances with the dispersion characteristics of equatorially trapped shallow water Kelvin modes (Takayabu 1994; Wheeler and Kiladis 1999, hereafter WK99). Variations in cloudiness associated with CCKWs peak along the latitude of the climatological intertropical convergence zone (ITCZ). The ITCZ generally is located between 5° and 15°N over the Atlantic basin, while it varies seasonally over Africa (Roundy and Frank 2004; Kiladis et al. 2009). Maximum zonal convergence associated with the CCKW occurs at 850 hPa and is located about 15° of longitude to the east of the outgoing longwave radiation (OLR) minima (Takayabu and Murakami 1991; Straub and Kiladis 2003a,b).

CCKWs over the tropical Atlantic and Africa have been presented in only a limited number of studies. Mekonnen et al. (2008) performed a study of a strong CCKW over tropical Africa. They demonstrated that rainfall within the vicinity of African topographic features (e.g., the GHs region and Ethiopia Highlands) increased considerably during the passage of the convectively active phase of a CCKW. Mounier et al. (2007) analyzed CCKWs over the Atlantic and Africa and found that the passage of the waves are preceded by low-level easterly wind anomalies and followed by low-level westerly wind anomalies, partly in phase with negative and positive geopotential height anomalies, respectively. They also state that most of the flow is zonal as predicted by theory, but strong monsoonal heating over West Africa does favor meridional southerly inflow, which leads to the enhancement of inland moisture advection along the Guinean coast at the location of the westerly low-level jet noted by Grodsky et al. (2003) and Pu and Cook (2010). Mounier et al. (2007) also demonstrate that MCSs traveling through the convective envelope of the CCKW over Africa often have higher amplitudes and tend to last longer. CCKWs have been shown to modify the background state and to intensify westward moving features traveling through its convectively active phase (Mekonnen et al. 2008). Therefore, it is natural to wonder if CCKWs can modulate tropical cyclone activity by enhancing westward propagating AEWs over the tropical Atlantic and/or by influencing the large-scale environment.

The role of CCKWs in tropical cyclogenesis has only been investigated in a handful of studies. Bessafi and Wheeler (2006) analyzed the relationship between CCKWs and tropical cyclogenesis over the Indian Ocean. They find a small yet statistically significant modulation of tropical cyclogenesis by quantifying the number of storms that formed when the active convection associated with the CCKW was located over the Indian Ocean. Frank and Roundy (2006) performed similar work on this relationship over all tropical Oceans. They suggest that there is a small preference for tropical cyclones to form in the negative OLR anomaly phase of a CCKW for all basins and conclude that CCKWs do not play a major role in tropical cyclogenesis. Since then, Roundy has reversed this view (P. Roundy 2011, personal communication). The technique applied by Roundy and Frank (2004) was not capable of accurately diagnosing the relationship between tropical cyclogenesis and CCKWs. This technique involved averaging Kelvin filtered OLR anomalies over the set of all dates when a tropical cyclone was named. Therefore, only a low-amplitude signal was retained, giving the appearance that the relationship between CCKWs and tropical cyclogenesis was minor. Schreck and Molinari (2011) have recently shown that a series of CCKWs embedded within the convectively active phase of the Madden–Julian oscillation (MJO) was largely responsible for the genesis of Typhoons Rammasun and Chataan (2002). Along with modifying the low-level wind field, this series of CCKWs diabatically generated an enhanced strip of PV that broke into two vortices that eventually formed Rammasun and Chataan.

This paper will investigate the role played by a CCKW in the genesis of Tropical Storm Debby in 2006. The focus will be on the development of Tropical Storm Debby as a case study highlighting a CCKW–AEW interaction. A companion paper, Ventrice et al. (2012), highlights the impact of strong CCKWs on the large-scale environmental conditions over the tropical Atlantic that is associated with tropical cyclogenesis.

The present paper is structured as follows. Section 2 discusses datasets and methodology. Section 3 investigates the genesis of Debby focusing on the evolution of the precursor AEW interacting with the diurnally varying convection over the GHs region. Section 3 analyzes the convective influence of CCKWs over the tropical Atlantic and African regions and considers the role of a strong CCKW on the development of Tropical Storm Debby. Section 4 investigates the climatological role of CCKWs on tropical cyclogenesis over the MDR. Finally, Section 5 includes a discussion and final comments.

2. Data and methodology

The European Centre for Medium-Range Weather Forecasts (ECMWF) Interim Re-Analysis (ERA-Interim) dataset was used to investigate the different synoptic evolutions of both the tropical cyclogenesis case study and the composite CCKW analysis (Simmons et al. 2007). This dataset covers the period 1989 to present and has a horizontal resolution of 1.5°. The AEW tracking method developed in Berry et al. (2007) was applied to the ERA-Interim data to objectively isolate trough axes of individual AEWs and locate the mean position of the AEJ.

Geostationary earth orbit IR data from the Climate Prediction Center (CPC) merged IR dataset was used to view the diurnal cycle of convection over the GHs region and the development of Tropical Storm Debby (Janowiak et al. 2001). This dataset is a composite of all geostationary earth-orbiting IR ($\sim$11 μm) images from the Multifunctional Transport Satellite [MTSAT; formerly the geostationary meteorological satellite], Geostationary Operational Environmental Satellite (GOES), and Meteosat satellites. Zenith angle corrections are used to match brightness temperatures away from the respective subsatellite points. The data are made available at 4-km spatial resolution every 30 min.

Tropical rainfall information was provided by the TRMM Multisatellite Precipitation Analysis (TMPA; TRMM product 3B42; Huffman et al. 2007). This dataset merges precipitation estimates from passive microwave sensors on a set of low-earth-orbiting satellites. The precipitation estimates are calibrated using global analyses of monthly rain gauge data. This dataset is made available from 1998 to the present on 3-hourly 0.25° latitude–longitude grids. The data have been averaged to 6-hourly 1° latitude–longitude grids to improve computational efficiency. By averaging the data onto a coarser grid, the missing data were interpolated bilinearly in space and linearly in time from the surrounding values. Less than 6% of the entire original 0.25° dataset contained a limited number of missing values, which were found to be caused by missing geostationary IR coverage over the Indian Ocean before June 1998 (Huffman et al. 2007).

Convection associated with CCKWs is explored using the National Oceanic and Atmospheric Administration's (NOAA) daily averaged interpolated OLR dataset, having a horizontal gridded resolution of 2.5° (Liebmann and Smith 1996). To support the analysis of CCKWs, wavenumber–frequency filtering was applied to the daily averaged NOAA interpolated OLR dataset following the methodology of WK99. CCKW filtering was performed with a period range of 2.5–20 days, with eastward wavenumbers 1–14. The filter is constrained by the Kelvin wave dispersion curves for equivalent depths of 8–90 m. This methodology has been demonstrated similarly in Straub and Kiladis (2002) and Mekonnen et al. (2008). In short, this methodology decomposes a field of data into wavenumber–frequency components for eastward moving wave disturbances. Before the decomposition, the data are detrended and the ends of the time series are tapered to zero to control spectral leakage (see WK99 for additional details). A time series was developed based on a selected grid point over the eastern tropical Atlantic (10°N, 15°W) selecting all days where the minimum Kelvin-filtered OLR anomalies were less than -1.5 standard deviations in magnitude during the 1989–2009 June–September (JJAS) seasons. A total of 142 CCKWs were objectively identified using this methodology. Lags were then used on this time series in order to examine propagating characteristics. For clarification, "day 0" is when the minimum Kelvin filtered OLR anomaly moves over the selected base point.

Anomalies for all composited fields were constructed as differences from the long-term mean and the first four harmonics of the seasonal cycle. Bootstrap random resampling tests with 1000 iterations were used for statistical significance testing on all anomalies (e.g., Roundy and Frank 2004). These tests were applied by constructing a number of samples equal in size to the anomaly dataset, which is obtained by randomly drawing a new set of anomalies with replacement from the original dataset and binning the anomalies for each randomly drawn set.

An analysis of tropical cyclogenesis events during 1979–2009 was performed using the National Climatic Data Center's (NCDC's) International Best Track Archive for Climate Stewardship (IBTrACS) v3 dataset (Knapp et al. 2010). The genesis of all tropical cyclones is binned relative to when OLR anomalies associated with the composite convectively active phase of the CCKW reached a level that was negative at the 95% significance level. A bootstrap resampling test was performed for statistical significance. To investigate the relationship between CCKWs and tropical cyclogenesis, tropical cyclogenesis is limited to only within the MDR (see section 4).

3. The influence of convection generated by the Guinea Highlands region on the development of Tropical Storm Debby

a. *The evolution of the African easterly wave associated with Tropical Storm Debby*

The evolution of the pre-Debby AEW is highlighted in Fig. 2. Key diagnostics include the 650-hPa PV, IR brightness temperature, and the mean location of the AEJ and AEW trough axes. The initiation of the pre-Debby AEW occurred after the generation of a strong MCS on 18 August over West Africa (10°–17°N, 0°–5°E; Fig. 2b) and is consistent with the triggering hypothesis discussed in Thorncroft et al. (2008). It is difficult to observe the AEW trough axis at this time because of the overall weak characteristics of the AEW. On 19 August, the midlevel circulation began to intensify as the AEW propagated westward over tropical Africa (Fig. 2c). Convection was observed on 19 August over Senegal, downstream of the AEW trough axis, consistent with the observations of previous AEW composite studies (e.g., Carlson 1969a,b; Reed et al. 1977; Payne and McGarry 1977; Duvel 1989; Diedhiou et al. 1999; Kiladis et al. 2006).

On 20 August, the AEW trough reached the longitude of the GHs region (Fig. 2d). At this time, the peak value of PV associated with the AEW was 0.3 PV units (PVU; 1 PVU = 10^{-6} K m^2 kg^{-1} s^{-1}). On 21 August, convection was more confined to the AEW trough axis (Fig. 2e). This location of convection resulted in an intensification of the midlevel PV, with the PV maximum of 0.6 PVU located behind the AEW trough axis. Six hours later at 0000 UTC 21 August, the NHC classified the pre-Debby AEW as a tropical cyclone. On 22 August, the tropical cyclone tracked northwest over the eastern tropical Atlantic; well-defined rainbands exist to the east of the tropical cyclone. During the intensification of the pre-Debby AEW, the 850-hPa meridional wind associated

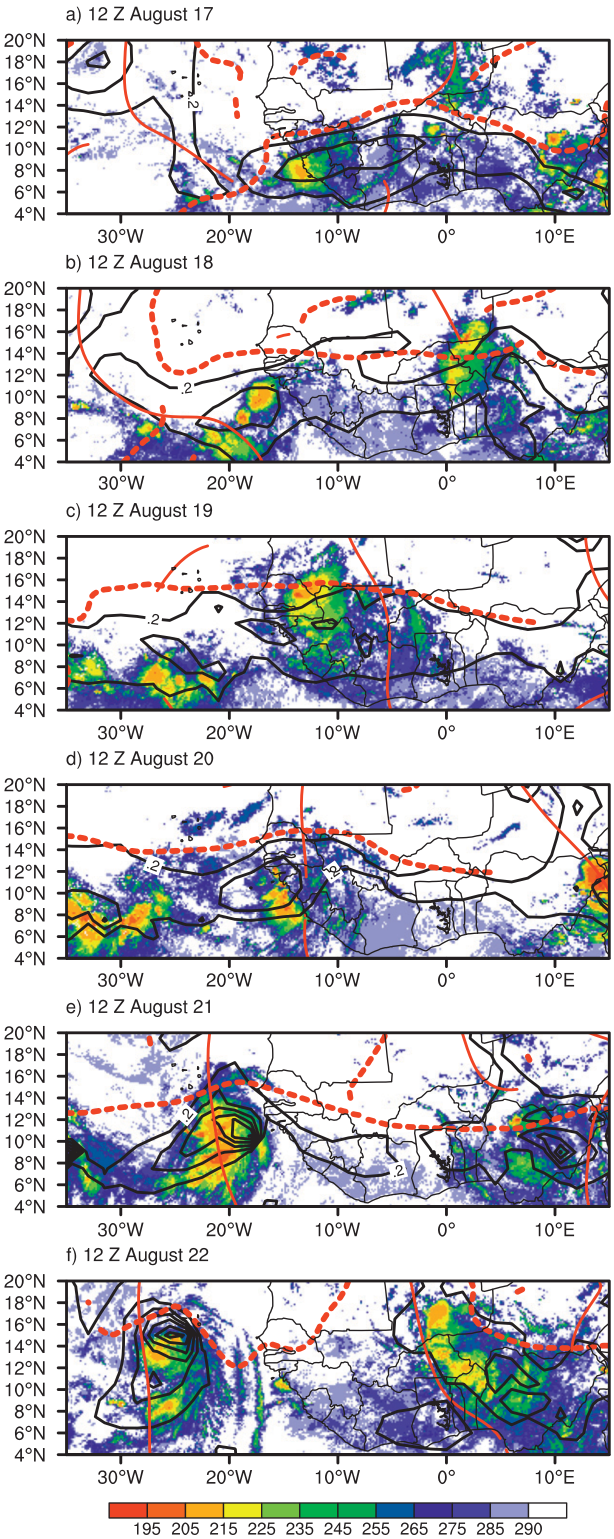

FIG. 2. The evolution of the pre-Debby AEW. Brightness temperature is shaded and 650-hPa PV is contoured (black). AEW trough axes are identified as north–south-oriented solid lines (red) and the mean position of AEJ is identified by the dashed line (red). Shade interval is 10 K; contours begin at 0.2 PVU; contour interval is 0.1 PVU.

with the low-level circulation of the AEW more than doubled from 2.5 m s^{-1} on 0000 UTC 20 August to greater than 5 m s^{-1} on 0000 UTC 21 August after propagating over the GHs region (not shown). As will be shown in the following subsections, this development likely had contributions from convection generated downstream of the GHs during the time of the AEW passage (section 3c) and the enhancement of convection by a strong CCKW (section 3e).

b. *Diurnal cycle of convection over the Guinea Highlands region*

Figure 3 shows the exceedance frequency of pixels less than 233 K for August 1998–2009. This provides an approximate estimation of the coherent diurnal cycle of rainfall (e.g., Duvel 1989; Mounier et al. 2007; Nguyen and Duvel 2008). There are two regions of elevated terrain near the coast of West Africa that compose the GHs region (recall Fig. 1). The taller, northernmost topographic feature (10°–12°N, 10°–13°W) is the Fouta Djallon Highlands (FDHs). The FDHs have a climatological daily rainfall rate of 8–12 mm day^{-1}. The southeasternmost topographic feature (7°–10°N, 7°–11°W) is the Nimba Range. The Nimba Range has a slightly lower climatological daily rainfall rate of 6–10 mm day^{-1}.

The diurnal cycle of convection over these regions is as follows. At 0300 UTC, the strongest convective signals are located in two regions, northwest of the FDHs and just off the coast of West Africa (Fig. 3a). A northwest–southeast-oriented line of convection is located over the extreme eastern Atlantic next to the coast. During the next 3 h (0600 UTC), the continental convection to the northwest of the GHs region weakens (Fig. 3b). The northwest–southeast-oriented line of oceanic convection is strikingly enhanced at this time. At 0900 UTC, the strongest convective activity continues to move westward over the ocean, slightly increasing in frequency (Fig. 3c). The convective signal over the continent continues to weaken.

At 1200 UTC, the convective activity over the continent is at a minimum while convection over the ocean remains pronounced (Fig. 3d). The reduction of cloudiness increases daytime solar heating reaching the surface, warming the land and destabilizing the boundary layer. The maximum oceanic convection begins to decrease and shift slightly westward by 1500 UTC. At this time, a new convective signal begins to appear over the coastal terrain downstream of the GHs region (Fig. 3e). This convective signal later grows in amplitude and extends across the entire continental–coastal terrain at 1800 UTC (Fig. 3f). A 233-K exceedance signal greater than 25% occurs over and downstream of the FDHs with a second, more localized area over the Nimba Range.

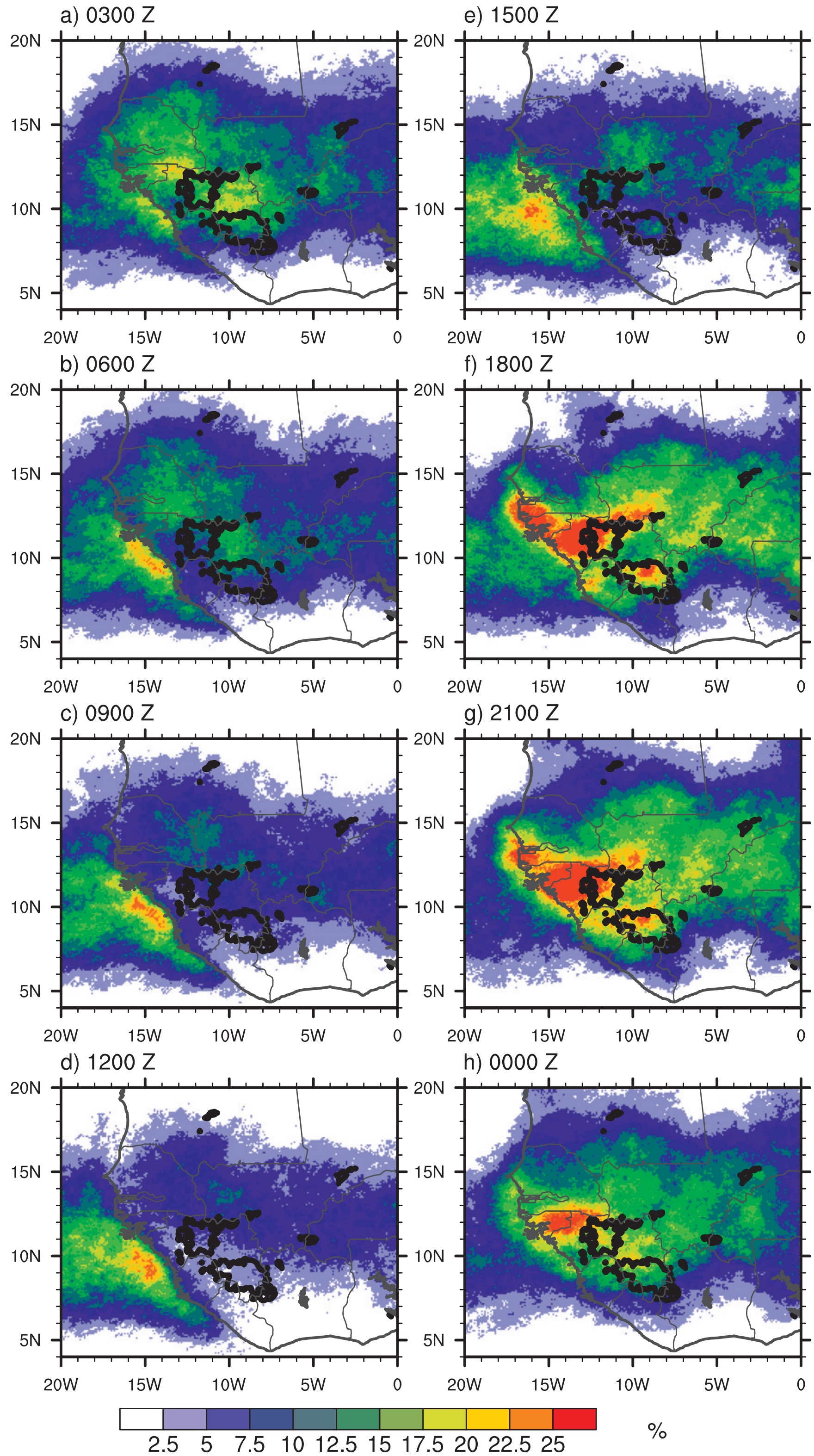

FIG. 3. August 1989–2009 hourly averaged 233-K exceedance frequency for every 3 h. Shading represents an estimation of the percentage of time a cloud is precipitating. Shade interval is 2.5%.

This convective pattern suggests that the elevated topography in this region acts to strongly influence the diurnal cycle of convection there. During the evening hours (2100–0000 UTC), the convective signal over the ocean continues to weaken considerably while the convective signal over the continent remains prominent (Figs. 3g,h).

In summary, convection most frequently occurs between 0000 and 1200 UTC over the eastern tropical Atlantic, in close proximity to the coast of West Africa. This oceanic convective signal is manifested by both (i) propagating MCSs that were either preexisting or directly generated over (or downstream) of the GHs topography and (ii) morning convection generated directly over the ocean. A transition from oceanic dominated convection to continental dominated convection occurs between 1500 and 1800 UTC (Fig. 3e).

c. The interaction between the convection generated by the Guinea Highlands region and the pre-Debby African easterly wave

Figure 4 shows the CPC IR brightness temperature on 0300 UTC 20 August through 0000 UTC 21 August 2006, the time of the AEW passage. The AEW trough axis and AEJ location are only plotted every 6 h because of the time resolution of the ERA-Interim dataset. This figure indicates that the diurnally varying convection generated within the vicinity of the GHs on 20 August was very similar to the coherent evolution described above and that this contributed to the intensification of the pre-Debby AEW leaving the coast of West Africa.

During the early morning hours (0300–0900 UTC), convection was generated directly off the coast of West Africa over the eastern tropical Atlantic similar to the coherent diurnal cycle (Figs. 4a–c). Between 0900 and 1200 UTC, the convection extended slightly northward over the ocean but was still very clearly tied to the coast (Figs. 4c,d). At 1200 UTC, a clearing along the coastal terrain was observed as the previous day's convection weakened (cf. Fig. 4d). This clearing occurred ahead and along the AEW trough axis, suggesting that the forcing from the diurnal cycle of convection was greater than that of the AEW. By 1500 UTC, convection began over the land close to the coast directly where the clearing of cloudiness was observed earlier (Fig. 4e). At 1800 UTC, deep convection associated with MCSs formed directly downstream of the FDHs (Fig. 4f). These MCSs occurred within the vicinity of the AEW trough axis and through the generation of low-to-mid level PV, and the AEW would be expected to strengthen at this time. At 2100 UTC, the convection associated with the MCSs intensified and extended northwestward (Fig. 4g). At this time, there are two large-scale convective features. There is a large MCS over the coast of Senegal and a second MCS over the eastern tropical Atlantic. The oceanic MCS was linked to the convection generated during the early morning. This MCS differs from the coherent diurnal cycle since it remained prominent during the afternoon, which is presumably associated with the forcing from the AEW. The second MCS was linked to the afternoon induced convection over land near the FDHs. This MCS occurred during a time consistent with the generation of new convection in the coherent diurnal cycle. Figure 4 suggests that the combined effects of the southerly flow associated with the circulation of the pre-Debby AEW and the topographic influence provided by the FDHs played a critical role in organizing this MCS (e.g., Chiao and Jenkins 2010). Between 0000 and 1200 UTC 21 August, the convection once initiated over the land merged with the active convection over the ocean, marking the early stages of tropical cyclogenesis.

The initial intensification of the pre-Debby AEW on 20 August occurred after interacting with the diurnally varying convection generated downstream of the GHs region. Convection was observed over the eastern Atlantic during the early morning hours of 20 August, consistent with exceedance frequency composites (cf. Figs. 3a–d). According to Zawislak and Zipser (2010), the MCS embedded within the oceanic convection just off the coast of West Africa possessed a similar magnitude to the afternoon triggered MCS on 20 August. Recall that this MCS over the ocean defied the coherent diurnal cycle of convection by maintaining its structure during a time of day when convection is on average suppressed over the ocean. It is likely that the synoptic forcing by the intensifying AEW influenced the development of both strong MCSs. This idea is consistent with Gray and Jacobson (1977), who found that the diurnal cycle is more evident within more intense deep convective systems. McGarry and Reed (1978) confirmed this result using the Global Atmospheric Research Program (GARP) Atlantic Tropical Experiment (GATE) array.

d. The convective influence of Kelvin waves over the tropical Atlantic and Africa

Composites of strong CCKWs over the tropical Atlantic and West Africa are calculated by averaging fields of unfiltered OLR anomalies, Kelvin filtered OLR anomalies, and 200-hPa wind anomalies over the set of dates composing the CCKW index (Fig. 5). Day 0 is defined to be when the composited minimum Kelvin filtered OLR anomaly is located over the base point (10°N, 15°W), chosen to be close to the West African coast. Consistent with previous studies, this figure clearly highlights eastward progression of negative OLR anomalies within the

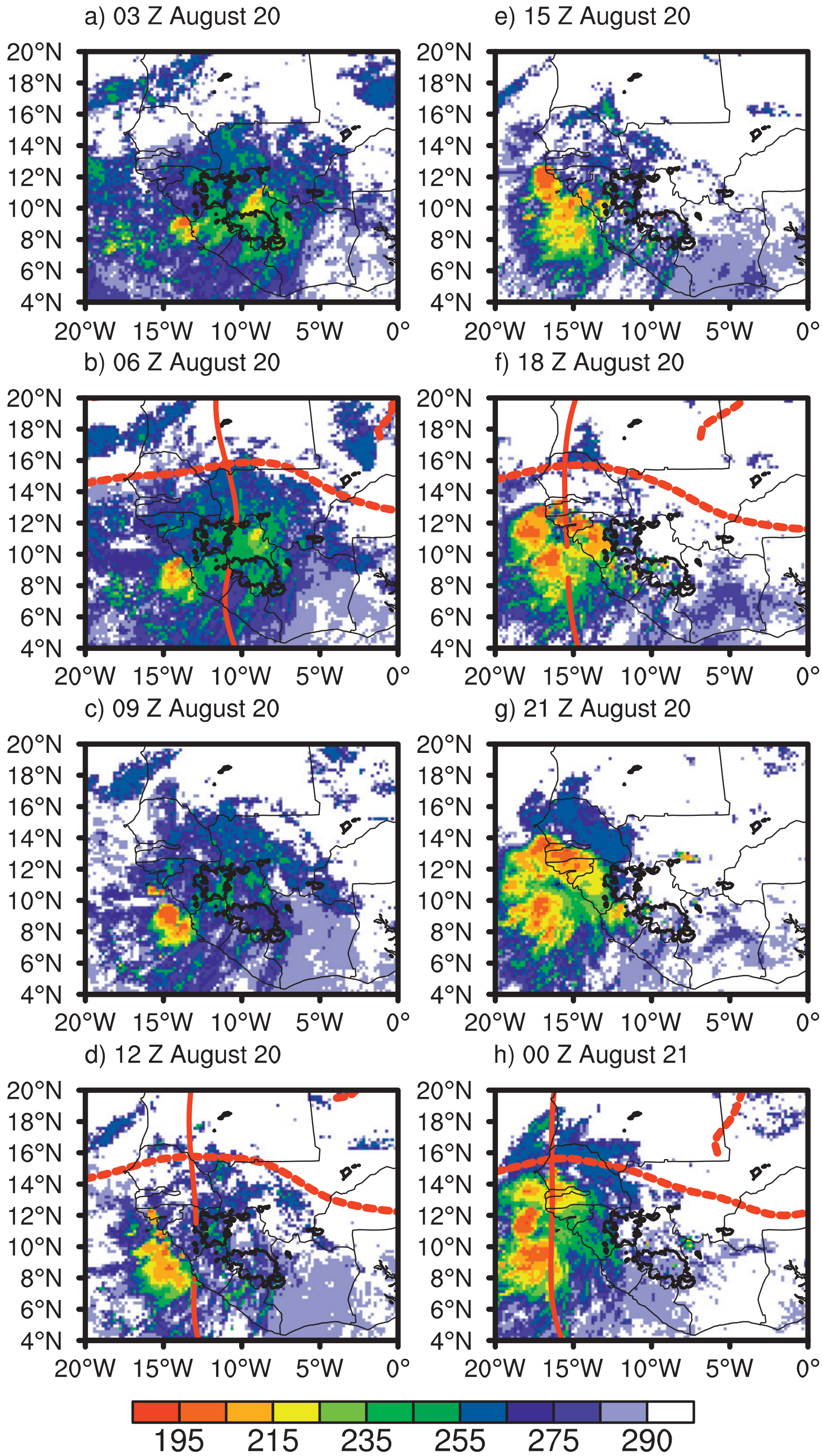

FIG. 4. Brightness temperature (shaded) highlighting the interaction between the pre-Debby AEW and the diurnal cycle of convection beginning at 0300 UTC 20 Aug and ending on 0000 UTC 21 Aug 2006 for every 3 h. The AEW trough axis is identified by the north–south-oriented line (red) and the AEJ is identified by the zonally oriented dashed line (red). Shade interval is 10 K.

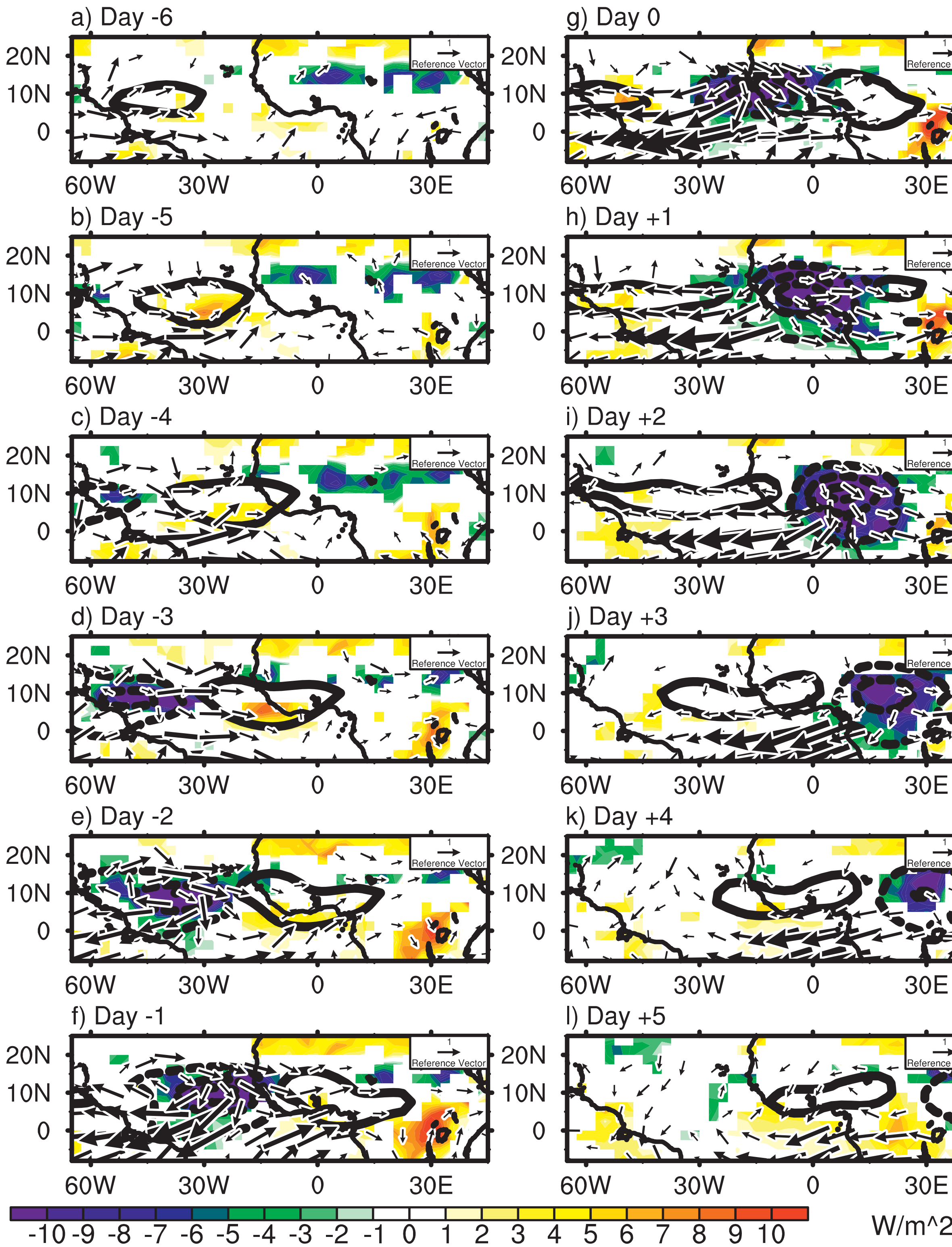

FIG. 5. NOAA daily averaged interpolated unfiltered OLR anomalies averaged over each CCKW lag. OLR anomalies statistically different than zero at the 95% level are shaded. Kelvin filtered OLR anomalies are contoured if statistically different than zero at the 95% level. Negative Kelvin filtered OLR anomalies are dashed. Vectors represent 200-hPa wind anomalies only showing magnitudes greater than 0.5 m s^{-1}. Shade interval is 1 W m^{-2}; contours begin at $\pm$3 W m^{-2} and the contour interval is 6 W m^{-2}; reference wind vector is 1 m s^{-1}.

composited convectively active phase of the CCKW over the tropical Atlantic and Africa.

The convectively suppressed phase of the composited CCKW (solid black contour) moves eastward ahead of the convectively active phase (dashed black contour), reducing local convection over the Atlantic ITCZ and tropical African regions. The convectively active phase of the CCKW progresses eastward, locally enhancing convection. A second convectively suppressed phase of the CCKW follows the convectively active phase. This "suppressed–active–suppressed" convective pattern associated with the CCKW travels eastward with an average phase speed of roughly 15 m s^{-1}. This phase speed is consistent with the 12–18 m s^{-1} observed CCKW phase speeds over the Indian Ocean (e.g., Dunkerton and Crum 1995; Roundy 2008), the western Pacific (e.g., WK99), the eastern Pacific (e.g., Straub and Kiladis 2002), and over West Africa (e.g., Mounier et al. 2007). Kiladis et al. (2009) attributes these slower than theoretical phase speeds to the reduced effective static stability of the atmosphere, which is associated with condensational heating and cooling canceling out most, but not all, of the temperature change linked to vertical motion.

Off-equatorial invigorated convection is collocated with the convectively active phase of the CCKW between day −2 and day +1 over the eastern Atlantic and GHs region (Figs. 5e–g). The enhanced convective signature associated with the CCKW is later located over tropical Africa between day +1 and day +4 (Figs. 5h–k). The off-equatorial convective signature is consistent with the location of the warmest sea surface temperatures (SSTs) in this region during the boreal summer. Near the equator itself, climatologically cold SSTs within the equatorial Atlantic cold tongue prevent deep convection from occurring there. This off-equatorial convective signature of the CCKW occurs similarly in the eastern Pacific, where the east Pacific cold tongue is present (Straub and Kiladis 2002).

Along with a coherent eastward moving convective signature, CCKWs also possess a coherent wind structure that progresses eastward with the wave. Emphasis will be given to the upper-level wind structure of the CCKW here, but it is acknowledged that CCKWs have a lower-level wind structure that is generally opposite to the flow in the upper troposphere (see Mounier et al. 2007; Roundy 2008). The upper-level wind pattern associated with the composited CCKW over the tropical Atlantic is similar to the theoretical dry Kelvin wave solution. Near the equator, upper-level westerly wind anomalies occur ahead of the minimum Kelvin filtered OLR anomaly. These upper-level westerly wind anomalies extend eastward through the leading convectively suppressed phase. Upper-level easterly wind anomalies are observed behind the minimum Kelvin filtered OLR anomaly and extend westward through the second suppressed phase. This anomalous wind pattern highlights large-scale upper-level wind divergence and is consistent with the deep convection that composes the convectively active phase of the CCKW. To the north of the equator, meridional wind anomalies compose a large portion of the upper-level wind structure of the composited CCKW. On day −2, a broad area of anomalous anticyclonic wind flow is collocated with the convectively active phase of the CCKW over the central Atlantic ITCZ (Fig. 5e). These winds are likely a response to the off-equatorial heating from convection at this time (e.g., Ferguson et al. 2009; Dias and Pauluis 2009). On day −1, the anomalous broad upper-level anticyclonic circulation shifts eastward with the convectively active phase of the CCKW (Fig. 5f). One day later (day 0), this anomalous anticyclonic circulation becomes less coherent, but anomalous easterly-northeasterly flow is evident over the entire equatorial Atlantic and anomalous westerly flow is over West Africa (Fig. 5f). This anomalous upper-level wind divergence pattern progresses eastward with the convectively active phase of the CCKW during the later lags (Figs. 5g–l).

e. *The Kelvin wave associated with the genesis of Tropical Storm Debby*

The superposition of a strong CCKW and the pre-Debby AEW occurred over the eastern tropical Atlantic on 21 August. This exceptional CCKW was associated with a 2σ negative Kelvin filtered OLR anomaly, ranking the wave within the strongest 5% of all JJAS (1979–2009) CCKWs over the selected base point. A time–longitude plot of unfiltered OLR anomalies overlaid with only negative Kelvin filtered OLR anomalies suggests that this CCKW was nondispersive in nature, making at least one circuit around the globe (Fig. 6). This CCKW is associated with a coherent eastward progression of negative Kelvin filtered OLR anomalies (dashed contours) beginning over the east Pacific (120°W) on 14 August and ending over the central Pacific on 6 September (180°). For most of this track over the Atlantic and West Africa, unfiltered negative OLR anomalies progress eastward with the Kelvin filtered negative OLR anomalies. The negative Kelvin filtered OLR anomalies associated with the strong CCKW that influenced the genesis of Debby do not connect to the area of negative Kelvin filtered OLR anomalies back over the eastern Pacific on 16 August. While the negative Kelvin filtered OLR anomalies suggest that the CCKW associated with Debby is different from the upstream CCKW over the central east Pacific (130°–140°W) during 14 and 15 August, the upper-level dynamical signature of these CCKWs is characterized by

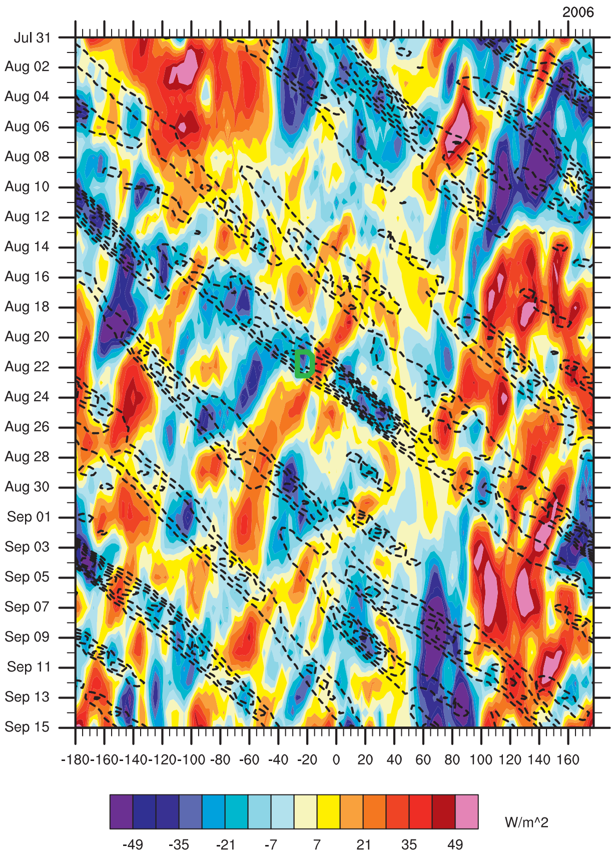

FIG. 6. A time–longitude plot averaging unfiltered OLR anomalies (shaded) and only negative Kelvin filtered OLR anomalies (dashed black lines) in the 7.5°–12.5°N latitude band. The green "D" represents the location where Debby became a named tropical cyclone. Contours begin at -3 W m^{-2} and the contour interval is -5 W m^{-2}; shade interval is 7 W m^{-2}.

more of a continuous signature (not shown). Therefore, these two areas of negative Kelvin filtered OLR anomalies are likely associated with the same CCKW. This result suggests that the CCKW associated with the genesis of Debby originated much farther west over the Indian Ocean (80°E) on 3 August. A detailed synoptic view of the interaction between the strong CCKW and the pre-Debby AEW is now highlighted in Fig. 7.

Because of the complexity of this figure, only the convectively active phase of the CCKW is discussed. On 18 August, the convectively active phase of the CCKW was expressed north of the equator over South America (Fig. 7a). At this time, the pre-Debby AEW was located roughly near the Greenwich meridian. The first sign of enhanced convection along the Atlantic ITCZ associated with the CCKW was on 20 August over 5°–10°N, 25°–35°W (Fig. 7c). The amplification of negative OLR anomalies over the MDR occurred during the superposition between a pre-existing AEW (pre-Ernesto) and the convectively active phase of the CCKW. Negative OLR anomalies associated with the pre-Ernesto AEW grew in horizontal area, extending over 0°–10°N, 25°–60°W on 21 August (Fig. 7d). This AEW later formed into a tropical depression near the Lesser Antilles on 24 August (Fig. 7g).

By 21 August, negative OLR anomalies associated with the CCKW were observed over the eastern tropical Atlantic, highlighting the initial interaction between the pre-Debby AEW (the north–south-oriented black line represents the AEW trough) and the CCKW (Fig. 7d). Eighteen hours later, the AEW formed into a tropical cyclone. On 22 August, the tropical cyclone intensified still within the convectively active phase of the CCKW (Fig. 7e). Note that the suppression of convection over West Africa east of Debby is located within the convectively active phase of the CCKW and is associated with the local suppression forced by a preexisting westward moving AEW.

Convection associated with Tropical Storm Debby weakened on 23 August after the passage of the convectively active phase of the CCKW (Fig. 7f). The suppression of convection over Tropical Storm Debby at this time has been related to its northwestward track into unfavorable conditions associated with a strong Saharan air layer (SAL; see Zipser et al. 2009). This suppression might also be associated with an interaction with the convectively suppressed phase of the CCKW (not shown).

During the subsequent days following the genesis of Debby, the convectively active phase of the CCKW progressed eastward over tropical Africa and provided an environment favorable for deep convection (Figs. 7f–h). On 25 August, the negative OLR anomalies associated with the CCKW are observed to extend over 30° of longitude over Africa, highlighting the significant role of the CCKW on African convection (Fig. 7h).

The focus is now on the anomalous upper-level wind field associated with the passage of the CCKW. Upper-level westerly wind anomalies were over the equatorial Atlantic, ahead of the convectively active phase of the CCKW on 18 August (Fig. 7a). Anomalous upper-level anticyclonic flow developed over the tropical Atlantic (centered over 10°N, 37°W) on 21 August during the superposition between the convectively active phase of the CCKW and the pre-Ernesto AEW (Fig. 7d). This anomalous anticyclonic circulation was also demonstrated in the CCKW composites, suggesting that this is a robust feature of CCKWs (recall Figs. 5e,f). Later on 21 August, anomalous equatorial easterly flow was to the west of the minimum Kelvin filtered OLR anomaly, with anomalous equatorial westerly flow to the east (Fig. 7e). This anomalous upper-level wind pattern over the eastern tropical Atlantic demonstrates that the CCKW strongly

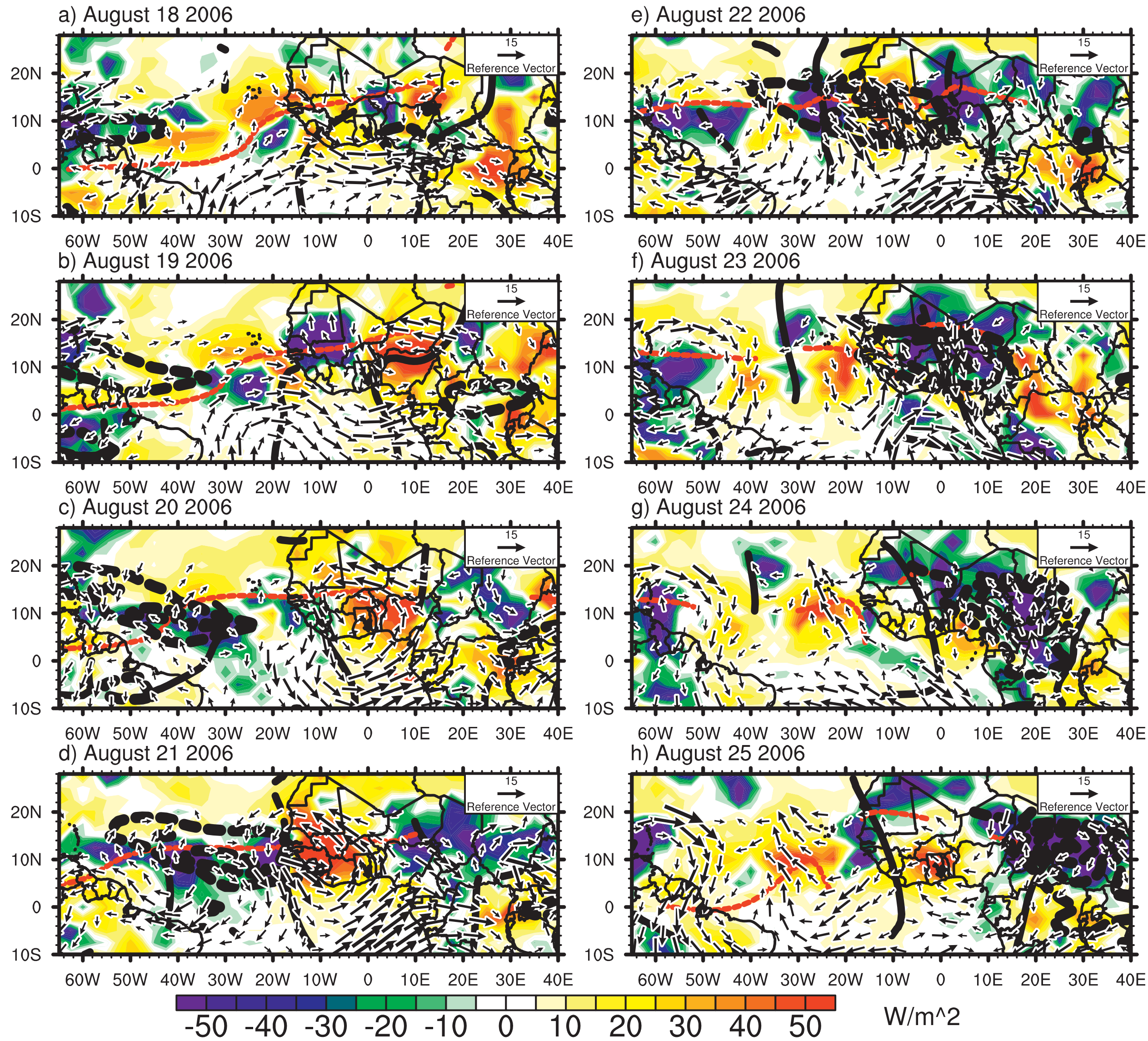

FIG. 7. The interaction between the pre-Debby AEW and a strong CCKW (21–22 Aug 2006). Shading is unfiltered OLR anomalies. Black dashed contours are negative Kelvin filtered OLR anomalies. South–north-oriented black lines highlight individual AEW trough axes. The red dashed line identifies the mean location of the AEJ. Vectors represent 200-hPa wind anomalies only showing magnitudes greater than 5 m s^{-1}. Shade interval is 10 W m^{-2}; contours begin at -10 W m^{-2} and the contour interval is -5 W m^{-2}; reference wind anomaly vector is 15 m s^{-1}.

contributed to the increased upper-level divergence over the eastern Atlantic. Further, anomalous northerly winds developed over the eastern tropical Atlantic during the passage of the convectively active phase of the CCKW. These anomalous northerly winds were most evident during the superposition between the CCKW and the pre-Debby AEW on 21–22 August, suggesting that the CCKW increased both the convection and convective outflow of the pre-Debby AEW. These anomalous northerly winds over the eastern Atlantic are also demonstrated during the passage of the convectively active phase of the composited CCKW (see Figs. 5f,g).

The upper-level wind structure of the CCKW was less coherent over tropical Africa. Between 22 and 24 August, the upper-level wind anomalies over Africa within the convectively active phase of the CCKW are mostly meridionally oriented (Figs. 7e–g). This anomalous wind pattern is inconsistent with the composited CCKW upper-level wind structure and might result from complex interactions occurring over Africa on different spatial and temporal scales that were not associated with the CCKW (e.g., AEWs, equatorial Rossby waves, diurnally driven convection, etc.). In this particular case, the circulation of a preexisting, very large westward propagating

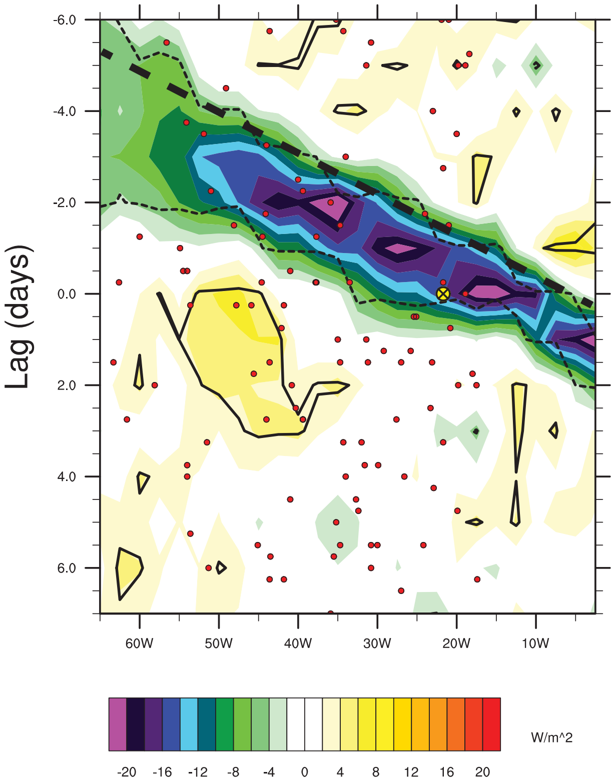

FIG. 8. A time–longitude plot of composited OLR anomalies averaged along 10°N during June–September 1979–2009. Composite unfiltered OLR anomalies are shaded. Positive OLR anomalies statistically different than zero at the 95% level are within the solid contour. Negative OLR anomalies statistically different than zero at the 95% level are within the dashed contour. The bold, larger dashed black line represents the beginning of "day 0" in Fig. 9. Tropical cyclogenesis within the MDR (5°–25°N, 65°–15°W) for any given lag is denoted by a red circle. Tropical Storm Debby is highlighted by the large yellow crossed circle. Shade interval is 2 W m^{-2}.

AEW destructively interfered with the upper-level wind structure of the CCKW between 22 and 24 August. However by 25 August, an anomalous upper-level anticyclonic circulation was reestablished within the convectively active phase of the CCKW over eastern Africa (Fig. 7h). Anomalous easterly winds extended westward over equatorial Africa and the equatorial Atlantic from the broad anomalous anticyclonic circulation over eastern tropical Africa, suggesting that the CCKW maintained its dynamical structure during the brief period of interference.

A summary of the sequence of events that resulted in the genesis of Tropical Storm Debby now follows. Enhanced, deep convection occurred over the pre-Debby AEW during the passage of the convectively active phase of the CCKW. This convection was found to be associated with two strong MCSs (see Zawislak and Zipser 2010). These MCSs were initially generated downstream of the GHs region on 20 August, in association with the dynamical forcing from the pre-Debby AEW. It has also been demonstrated that these high-amplitude MCSs intensified during the superposition between the convectively active phase of the CCKW and the pre-Debby AEW on 21 August. The influence of deep convection favored within the convectively active phase of the CCKW on the pre-Debby AEW aided the tropical cyclogenesis via increased latent release and PV generation (recall Fig. 2e). Given that this result is somewhat new in this region, the general relationship between CCKWs and tropical cyclogenesis is investigated over the MDR in the following section.

4. The influence of Kelvin waves on Atlantic tropical cyclogenesis

CCKWs might modulate tropical cyclogenesis over the MDR by directly amplifying westward propagating AEWs. To investigate the relationship between CCKWs and tropical cyclogenesis, Fig. 8 shows a time–longitude composite using the CCKW index of unfiltered OLR anomalies (shaded) and the locations of tropical cyclogenesis events occurring equatorward of 25°N. Generally, there is a low number of tropical cyclogenesis events observed between the leading convectively suppressed phase and the convectively active phase of the CCKW. Tropical cyclogenesis is more frequent within the convectively active phase of the CCKW (as is the case of Tropical Storm Debby; larger yellow crossed circle). However, tropical cyclogenesis becomes most frequent just after the passage of the convectively active phase of the CCKW. This increase of tropical cyclogenesis events occurs in the general area after the passage of the convectively active phase and during the initial passage of the second convectively suppressed phase.

To quantify the counts of tropical cyclogenesis events relative to the CCKW in daily intervals, Fig. 9 shows the number of tropical cyclogenesis events relative to the local passage of the CCKW's convectively active phase. The start of day 0 represents the transition to statistically significant unfiltered negative OLR anomalies associated with the CCKW over the entire MDR (slanted bold black dashed line on Fig. 8). One day prior to the convectively active phase of the CCKW (day −1), a minimum of tropical cyclogenesis is observed. This relatively reduced period of tropical cyclogenesis activity occurs after the passage of the leading convectively suppressed phase of the CCKW. A large increase in the number of tropical cyclogenesis events is observed between day −1 and day +2, the peak in tropical cyclogenesis frequency.

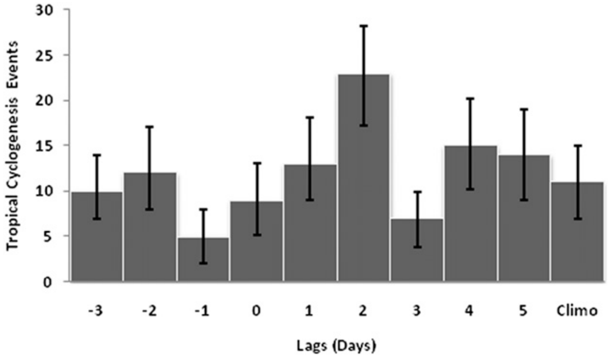

FIG. 9. Tropical cyclogenesis events over the MDR (5°–25°N, 15°–65°W) relative to the CCKW during June–September 1979–2009. Day 0 highlights the transition to statistically significant negative unfiltered OLR anomalies associated with the CCKW, or the easternmost side of the convectively active phase. The ''Climo'' lag represents the climatological number of tropical cyclogenesis events for an average daily lag. Error bars indicate the 90% confidence interval.

This peak is statistically different from the counts of tropical cyclogenesis events in four different lags (days −3, −1, 0, and +3) at the 95% level. Further, the count of tropical cyclogenesis events on day +2 is statistically different to climatology at the 90% level. This lead–lag relationship between the passage of the convectively active phase of the CCKW and the increased events of tropical cyclogenesis activity may occur because of a lag between convective enhancement over a tropical wave and the actual naming of a tropical cyclone. On the other hand, since the peak of tropical cyclogenesis events does not occur under the convectively active phase of the CCKW (day +2 occurs between the convectively active phase of the CCKW and the second convectively suppressed phase), the enhancement of tropical cyclogenesis activity might not occur from convective processes alone. We hypothesize that the CCKW may be impacting the large-scale environmental conditions associated with tropical cyclogenesis. This hypothesis will be explored in Ventrice et al. (2012).

5. Discussion and conclusions

Observations were presented of an initially weak AEW undergoing tropical cyclogenesis after interacting with the convective processes generated downstream of the GHs region, as well as interacting with an eastward propagating CCKW during the 2006 NAMMA field campaign. These observations present a new aspect of tropical weather variability over tropical Africa and tropical cyclogenesis variability over the tropical Atlantic.

CPC IR data indicate that the pre-Debby AEW interacted with the coherent diurnal cycle of convection generated over the GHs region. These daily convective processes enhanced the pre-Debby AEW as it propagated off the coast of West Africa. Early morning oceanic convection was observed prior to the passage of the pre-Debby AEW. This oceanic convection remained active during the afternoon hours, a time when convection is normally suppressed. During the passage of the pre-Debby AEW over the GHs region, deep afternoon convection generated directly northwest of the FDHs and occurred within the vicinity of the AEW trough, enhancing the AEW. On 21 August, the convectively active phase of the CCKW first interacted with the pre-Debby AEW just off the coast of West Africa (Fig. 6d). This was the same time that Zawislak and Zipser (2010) observed two of the strongest West African MCSs seen in the JJAS 1998–2007 TRMM climatology. These MCSs were initially generated by the interaction between the diurnal cycle of convection generated by the GHs region and the pre-Debby AEW. On 21 August, the minimum Kelvin filtered OLR value is located roughly 15° west of where the strong MCSs were observed by Zawislak and Zipser (2010). In addition from the forcing of the pre-Debby AEW, it seems likely that these strong MCSs were also influenced by the CCKW.

The genesis of Tropical Storm Debby occurred during the superposition between the convectively active phase of a strong CCKW and the pre-Debby AEW on 21–22 August. Tropical cyclogenesis occurred during the CCKW passage at 1800 UTC 21 August. Based on the analysis presented here, it is suggested that the CCKW modulated the wind field over the eastern tropical Atlantic prior to and during the passage of the pre-Debby AEW. The modulation of wind was demonstrated by investigating the upper-level winds, but CCKWs also influence winds in the lower troposphere. Anomalous low-level westerly wind anomalies are collocated with the convectively active phase of the CCKW, whereas anomalous low-level easterly winds are collocated within the leading convectively suppressed phase (not shown). Therefore, during the superposition of the convectively active phase of the CCKW and the pre-Debby AEW, one might expect an enhancement of the low-level westerly winds near the equator. Vizy and Cook (2009) found that the development of the pre-Debby AEW over the Cape Verde region was associated with a strong low-level westerly jet located just south of the 850-hPa vortex center. The acceleration of low-level westerly flow prior to tropical development has been found to be an influential mechanism in providing the external forcing (e.g., low-level cyclonic vorticity and large-scale vertical ascent) necessary for tropical cyclogenesis (e.g., Gray 1988, 1998; Lee et al. 1989; Briegel and Frank 1997). We suggest that this acceleration of low-level westerly flow prior to development of Debby had a strong contribution from the CCKW.

Vizy and Cook (2009) suggest that the AEW (pre-Ernesto) that preceded the pre-Debby AEW created a surge of low-level westerly flow that provided a favorable environment for the genesis of Debby. An alternative hypothesis is suggested here, highlighting the fact that both AEWs interacted with the same strong CCKW, a synoptic-scale feature that influenced the MDR roughly during the period 18–24 August. The superposition of the two different AEWs with the convectively active phase of the CCKW occurred over different regions of the MDR. The fact that Ernesto did not immediately form into a tropical cyclone after interacting with the CCKW on 20 August can be attributed to the presence of a strong SAL outbreak (Zipser et al. 2010). Ernesto later formed into a tropical cyclone on 24 August, after moving out of the SAL environment. Debby formed immediately into a tropical cyclone over the eastern Atlantic while interacting with the same CCKW but decayed soon after moving northwestward into a strong SAL outbreak (see Zipser et al. 2010). In contrast to this hypothesis, Braun (2010) and Sippel et al. (2011) find that subsidence associated with deep, dry convective mixing over the Sahara created the dry air over the eastern tropical Atlantic, which eventually lead to the decay of Debby.

A coherent relationship between tropical cyclogenesis over the MDR and CCKWs is also revealed from a climatological perspective. Tropical cyclogenesis is found to be significantly lower after the passage of the leading convectively suppressed phase of the CCKW. Tropical cyclogenesis becomes significantly more frequent two days after convection is initially excited by the CCKW. This relationship opposes the past work that suggest relatively minor relationships between tropical cyclogenesis and CCKWs (e.g., Frank and Roundy 2006; Schreck et al. 2011) and is quantified by counting the number of tropical cyclones that form relative to an eastward propagating CCKW.

To fully assess the influence of a CCKW passage on tropical cyclogenesis, an analysis of CCKWs within the large-scale environment is needed. Since a 2-day lag exists between the passage of the leading edge of the convectively active phase of a CCKW and the peak of tropical cyclogenesis frequency, there is a suggestion that CCKWs may alter large-scale environmental conditions over the MDR for a period of time after its passage in addition to enhancing convection. This analysis will be presented in Ventrice et al. (2012).

The genesis of Tropical Storm Debby (2006) might have been better anticipated if forecasters, in addition to being aware of the westward propagating AEW, had been aware of the high-amplitude eastward propagating CCKW over the tropical Atlantic. Being aware of this fact might have allowed forecasters to issue a more advanced warning in contrast to the 3-h warning that was provided by the Tropical Weather Outlook product. CCKWs impact tropical weather every day and it is strongly recommended that these waves be included in forecast discussions.

Acknowledgments. The authors would like thank NOAA CPC, NCEP, and the NASA TRMM program for providing the satellite data in the study. We extend our gratitude to NASA for the Grant NNX09AD08G that supported this research. We also express gratitude to Carl Schreck and Alan Brammer for their help with data analysis, to Paul Roundy for personal communications, and to all reviewers who have made insightful contributions toward the manuscript.

REFERENCES

Avila, L. A., and R. J. Pasch, 1992: Atlantic tropical systems of 1991. *Mon. Wea. Rev.,* **120,** 2688–2696.

Berry, G., and C. D. Thorncroft, 2005: Case study of an intense African easterly wave. *Mon. Wea. Rev.,* **133,** 752–766.

——, ——, and T. Hewson, 2007: African easterly waves during 2004—Analysis using objective techniques. *Mon. Wea. Rev.,* **135,** 1251–1267.

Bessafi, M., and M. Wheeler, 2006: Modulation of south Indian Ocean tropical cyclones by the Madden–Julian oscillation and convectively coupled equatorial waves. *Mon. Wea. Rev.,* **134,** 638–656.

Braun, S. A., 2010: Reevaluating the role of the Saharan air layer in Atlantic tropical cyclogenesis and evolution. *Mon. Wea. Rev.,* **138,** 2007–2037.

Briegel, L. M., and W. M. Frank, 1997: Large-scale influences on tropical cyclogenesis in the western North Pacific. *Mon. Wea. Rev.,* **125,** 1397–1413.

Carlson, T. N., 1969a: Synoptic histories of three African disturbances that developed into Atlantic hurricanes. *Mon. Wea. Rev.,* **97,** 256–276.

——, 1969b: Some remarks on African disturbances and their progress over the tropical Atlantic. *Mon. Wea. Rev.,* **97,** 716–726.

Chiao, S., and G. S. Jenkins, 2010: Numerical investigations on the formation of Tropical Storm Debby during NAMMA-06. *Wea. Forecasting,* **25,** 866–884.

Dias, J., and O. Pauluis, 2009: Convectively coupled waves propagating along an equatorial ITCZ. *J. Atmos. Sci.,* **66,** 2237–2255.

Diedhiou, A., S. Janicot, A. Viltard, P. de Felice, and H. Laurent, 1999: Easterly wave regimes and associated convection over West Africa and tropical Atlantic: Results from the NCEP/NCAR and ECMWF reanalysis. *Climate Dyn.,* **15,** 795–822.

Dunkerton, T. J., and F. X. Crum, 1995: Eastward propagating ~2- to 15-day equatorial convection and its relation to the tropical intraseasonal oscillation. *J. Geophys. Res.,* **100** (D12), 25 781–25 790.

Duvel, J. P., 1989: Convection over tropical Africa and the Atlantic Ocean during northern summer. Part I: Interannual and diurnal variations. *Mon. Wea. Rev.,* **117,** 2782–2799.

Ferguson, J., B. Khouider, and M. Namazi, 2009: Two-way interactions between equatorially trapped waves and the barotropic flow. *Chin. Ann. Math.,* **30B,** 539–568.

Frank, W. M., and P. E. Roundy, 2006: The role of tropical waves in tropical cyclogenesis. *Mon. Wea. Rev.,* **134,** 2397–2417.

Gray, W. M., 1988: Environmental influences on tropical cyclones. *Aust. Meteor. Mag.,* **36,** 127–139.

——, 1998: The formation of tropical cyclones. *Meteor. Atmos. Phys.,* **67,** 37–69.

——, and R. W. Jacobson Jr., 1977: Diurnal variation of deep cumulus convection. *Mon. Wea. Rev.,* **105,** 1171–1188.

Grodsky, S. A., J. A. Carton, and S. Nigam, 2003: Near surface westerly wind jet in the Atlantic ITCZ. *Geophys. Res. Lett.,* **30,** 2009, doi:10.1029/2003GL017867.

Hodges, K. I., and C. D. Thorncroft, 1997: Distribution and statistics of African mesoscale convective weather systems based on the ISCCP Meteosat imagery. *Mon. Wea. Rev.,* **125,** 2821–2837.

Hopsch, S. B., C. D. Thorncroft, K. Hodges, and A. Aiyyer, 2007: West African storm tracks and their relationship to Atlantic tropical cyclones. *J. Climate,* **20,** 2468–2483.

——, ——, and K. R. Tyle, 2010: Analysis of African easterly wave structures and their role in influencing tropical cyclogenesis. *Mon. Wea. Rev.,* **138,** 1399–1419.

Huffman, G. J., and Coauthors, 2007: The TRMM Multisatellite Precipitation Analysis (TMPA): Quasi-global, multiyear, combined-sensor precipitation estimates at fine scales. *J. Hydrometeor.,* **8,** 38–55.

Janowiak, J., P. A. Arkin, and M. Morrissey, 1994: An examination of the diurnal cycle in oceanic tropical rainfall using satellite and in situ data. *Mon. Wea. Rev.,* **122,** 2296–2311.

——, R. J. Joyce, and Y. Yarosh, 2001: A real-time global half-hourly pixel-resolution infrared dataset and its applications. *Bull. Amer. Meteor. Soc.,* **82,** 205–217.

Kiladis, G. N., C. D. Thorncroft, and N. M. J. Hall, 2006: Three-dimensional structure and dynamics of African easterly waves. Part I: Observations. *J. Atmos. Sci.,* **63,** 2212–2230.

——, M. C. Wheeler, P. T. Haertel, K. H. Straub, and P. E. Roundy, 2009: Convectively coupled equatorial waves. *Rev. Geophys.,* **47,** RG2003, doi:10.1029/2008RG000266.

Knapp, K. R., M. C. Kruk, D. H. Levinson, H. J. Diamond, and C. J. Neumann, 2010: The International Best Track Archive for Climate Stewardship (IBTrACS): Unifying tropical cyclone data. *Bull. Amer. Meteor. Soc.,* **91,** 363–376.

Kwon, H. J., and M. Mak, 1990: A study of the structural transformation of the African easterly waves. *J. Atmos. Sci.,* **47,** 277–292.

Laing, A. G., R. E. Carbone, V. Levizzani, and J. D. Tuttle, 2008: The propagation and diurnal cycles of deep convection in northern tropical Africa. *Quart. J. Roy. Meteor. Soc.,* **134,** 93–109.

Lee, C.-S., R. Edson, and W. M. Gray, 1989: Some large-scale characteristics associated with tropical cyclone development in the north Indian Ocean during FGGE. *Mon. Wea. Rev.,* **117,** 407–426.

Liebmann, B., and C. A. Smith, 1996: Description of a complete (interpolated) outgoing longwave radiation dataset. *Bull. Amer. Meteor. Soc.,* **77,** 1275–1277.

McGarry, M. M., and R. J. Reed, 1978: Diurnal variations in convective activity and precipitation during phases II and III of GATE. *Mon. Wea. Rev.,* **106,** 101–113.

Mekonnen, A., C. D. Thorncroft, and A. R. Aiyyer, 2006: Analysis of convection and its association with African easterly waves. *J. Climate,* **19,** 5405–5421.

——, ——, ——, and G. N. Kiladis, 2008: Convectively coupled Kelvin waves over tropical Africa during the boreal summer: Structure and variability. *J. Climate,* **21,** 6649–6667.

Mounier, F., G. N. Kiladis, and S. Janicot, 2007: Analysis of the dominant mode of convectively coupled Kelvin waves in the West African monsoon. *J. Climate,* **20,** 1487–1503.

Nguyen, H., and J. P. Duvel, 2008: Synoptic wave perturbations and convective systems over equatorial Africa. *J. Climate,* **21,** 6372–6388.

Payne, S. W., and M. M. McGarry, 1977: The relationship of satellite inferred convective active to easterly waves over West Africa and the adjacent ocean during phase III of GATE. *Mon. Wea. Rev.,* **105,** 413–420.

Pu, B., and K. H. Cook, 2010: Dynamics of the West African westerly jet. *J. Climate,* **23,** 6263–6276.

Reed, J. R., D. C. Norquist, and E. E. Recker, 1977: The structure and properties of African wave disturbances as observed during phase III of GATE. *Mon. Wea. Rev.,* **105,** 317–333.

Roundy, P. E., 2008: Analysis of convectively coupled Kelvin waves in the Indian Ocean MJO. *J. Atmos. Sci.,* **65,** 1342–1359.

——, and W. M. Frank, 2004: A climatology of waves in the equatorial region. *J. Atmos. Sci.,* **61,** 2105–2132.

Schreck, C. J., III, and J. Molinari, 2011: Tropical cyclogenesis associated with Kelvin waves and the Madden–Julian oscillation. *Mon. Wea. Rev.,* **139,** 2723–2734.

——, ——, and K. I. Mohr, 2011: Attributing tropical cyclogenesis to equatorial waves in the western North Pacific. *J. Atmos. Sci.,* **68,** 195–209.

Simmons, A., S. Uppala, D. Dee, and S. Kobayashi, 2007: ERA-Interim: New ECMWF reanalysis products from 1989 onwards. *ECMWF Newsletter,* No. 110, ECMWF, Reading, United Kingdom, 25–35.

Sippel, J. A., S. A. Braun, and C.-L. Shie, 2011: Environmental influences on the strength of Tropical Storm Debby (2006). *J. Atmos. Sci.,* **68,** 2557–2581.

Straub, K. H., and G. N. Kiladis, 2002: Observations of a convectively coupled Kelvin waves in the eastern Pacific ITCZ. *J. Atmos. Sci.,* **59,** 30–53.

——, and ——, 2003a: Extratropical forcing of convectively coupled Kelvin waves during austral winter. *J. Atmos. Sci.,* **60,** 526–543.

——, and ——, 2003b: The observed structure of convectively coupled Kelvin waves: Comparison with simple models of coupled wave instability. *J. Atmos. Sci.,* **60,** 1655–1668.

Takayabu, Y. N., 1994: Large-scale cloud disturbances associated with equatorial waves. Part I: Spectral features of the cloud disturbances. *J. Meteor. Soc. Japan,* **72,** 433–448.

——, and M. Murakami, 1991: The structure of super cloud clusters observed on 1–20 June 1986 and their relationship to easterly waves. *J. Meteor. Soc. Japan,* **69,** 105–125.

Thompson, R. M., Jr., S. W. Payne, E. E. Recker, and R. J. Reed, 1979: Structure and properties of synoptic-scale wave disturbances in the intertropical convergence zone of the eastern Atlantic. *J. Atmos. Sci.,* **36,** 53–72.

Thorncroft, C. D., and K. Hodges, 2001: African easterly wave variability and its relationship to Atlantic tropical cyclone activity. *J. Climate,* **14,** 1166–1179.

——, N. M. Hall, and G. K. Kiladis, 2008: Three-dimensional structure and dynamics of African easterly waves. Part III: Genesis. *J. Atmos. Sci.,* **65,** 3596–3607.

Ventrice, M. J., C. D. Thorncroft, and C. J. Schreck, 2012: Impacts of convectively coupled Kelvin waves on environmental conditions for Atlantic tropical cyclogenesis. *Mon. Wea. Rev.,* in press.

Vizy, E. K., and K. H. Cook, 2009: Tropical storm development from African easterly waves in the eastern Atlantic: A comparison of two successive waves using a regional model as part of NASA AMMA 2006. *J. Atmos. Sci.,* **66,** 3313–3334.

Wheeler, M., and G. N. Kiladis, 1999: Convectively coupled equatorial waves: Analysis of clouds and temperature in the wavenumber–frequency domain. *J. Atmos. Sci.,* **56,** 374–399.

Yang, G., and J. Slingo, 2001: The diurnal cycle in the tropics. *Mon. Wea. Rev.,* **129,** 784–801.

Zawislak, J., and E. J. Zipser, 2010: Observations of seven African easterly waves in the east Atlantic during 2006. *J. Atmos. Sci.,* **67,** 26–43.

Zipser, E. J., and C. Gautier, 1978: Mesoscale events within a GATE tropical depression. *Mon. Wea. Rev.,* **106,** 789–805.

——, and Coauthors, 2009: The Saharan air layer and the fate of African easterly waves—NASA's AMMA field study of tropical cyclogenesis. *Bull. Amer. Meteor. Soc.,* **90,** 1137–1156.